

Published in final edited form as:

Phys Med Biol. 2009 December 21; 54(24): 7315–7327. doi:10.1088/0031-9155/54/24/005.

A histology-based atlas of the C57BL/6J mouse brain deformably registered to *in vivo* MRI for localized radiation and surgical targeting

David Purger¹, Todd McNutt¹, Pragathi Achanta², Alfredo Quiñones-Hinojosa², John Wong¹, and Eric Ford^{1,3}

¹ Department of Radiation Oncology and Molecular Radiation Sciences, Johns Hopkins University, 401 North Broadway, Suite 1440, Baltimore, MD 21231, USA

² Department of Neurosurgery, Johns Hopkins University, Cancer Research Building II, 1550 Orleans Street, Room 247, Baltimore, MD 21231, USA

Abstract

The C57BL/6J laboratory mouse is commonly used in neurobiological research. Digital atlases of the C57BL/6J brain have been used for visualization, genetic phenotyping and morphometry, but currently lack the ability to accurately calculate deviations between individual mice. We developed a fully three-dimensional digital atlas of the C57BL/6J brain based on the histology atlas of Paxinos and Franklin (2001 *The Mouse Brain in Stereotaxic Coordinates* 2nd edn (San Diego, CA: Academic)). The atlas uses triangular meshes to represent the various structures. The atlas structures can be overlaid and deformed to individual mouse MR images. For this study, we selected 18 structures from the histological atlas. Average atlases can be created for any group of mice of interest by calculating the mean three-dimensional positions of corresponding individual mesh vertices. As a validation of the atlas' accuracy, we performed deformable registration of the lateral ventricles to 13 MR brain scans of mice in three age groups: 5, 8 and 9 weeks old. Lateral ventricle structures from individual mice were compared to the corresponding average structures and the original histology structures. We found that the average structures created using our method more accurately represent individual anatomy than histology-based atlases alone, with mean vertex deviations of 0.044 mm versus 0.082 mm for the left lateral ventricle and 0.045 mm versus 0.068 mm for the right lateral ventricle. Our atlas representation gives direct spatial deviations for structures of interest. Our results indicate that MR-deformable histology-based atlases represent an accurate method to obtain accurate morphometric measurements of a population of mice, and that this method may be applied to phenotyping experiments in the future as well as precision targeting of surgical procedures or radiation treatment.

1. Introduction

The mouse is one of the most widely used animals for modeling human neurobiology in the laboratory due to its relative similarity to humans and the vast amount of phenotypic information available about common inbred strains such as C57BL/6J via resources such as the Mouse Phenome Database (MPD; <http://phenome.jax.org/pub-cgi/phenome/mpdcgi>). To support such research, several groups have created three-dimensional (3D) atlases of the mouse brain. These atlases are important for a wide variety of applications, including visualization of neuroanatomical structures (e.g. Toga *et al* (1989)), genetic phenotyping

experiments (e.g. Bock *et al* (2006)) and interventional applications such as stem cell studies (Zhao *et al* 2008). Initial work was based on photographic digitization of printed, histology-derived atlases of rodent brains intended for surgical planning, such as Paxinos and Watson's rat brain atlas (1986, in Toga *et al* 1989); however, the finding that crude alignment of individual slides of the two-dimensional atlas yields a discontinuous 3D structure (Toga *et al* 1989) as well as possible inaccuracies of such an atlas from histological methods such as fixation argues against a purely histological approach to atlas construction, despite the potential for cellular-level resolution (2–5 μm). In addition, atlases such as Paxinos and Watson's rely on a single representative brain specimen and thus do not incorporate any anatomical variation across strains.

One approach that addresses the issue of variability between rodent subjects is the use of magnetic resonance imaging (MRI). Atlases of the mouse brain based on MRI data employ one of two approaches: MRI scans of *ex vivo* tissue at high resolution (e.g. 60 μm , Ková evi *et al* (2005); 47 μm , Ma *et al* (2005)) using long acquisition times and high-field strengths (e.g. 7 T and 18.5 h, Ková evi *et al* (2005); 17.6 T and 5.5 h, Ma *et al* (2005)) or *in vivo* MRI scans at typically lower resolution (e.g. 156 μm ; Bock *et al* 2006). A number of human studies (e.g. Eickhoff *et al* (2005), Amunts and Zilles (2001)) present a comparison of accuracy between *in vivo* MRI and histology or approaches based on deforming both histology atlases and individual subject MRI volumes to a standard brain space, but these methods lack the advantages of a deformable, three-dimensional atlas. No approach using rodents, to date, combines the high resolution of histology-based atlases with the convenience and ability to perform further studies of *in vivo* MR techniques.

Atlases of the mouse brain, to date, are usually used for visualization of anatomical structures, morphometric analysis and phenotyping experiments. These approaches are concerned mostly with gross anatomical differences between specimens, but another class of applications exists for which variations in the spatial location of the fine structure are critical and currently existing atlases are thus unsuited. One particular application of interest in our laboratory is the delivery of precision radiation beams to substructures in the brain. This application is enabled by a new generation of animal radiation devices capable of delivering x-ray beams as small as 0.5 mm diameter to rodent brains using on-board computed tomography (CT) guidance (Wong *et al* 2008). With this technology, it is possible to irradiate isolated regions or nuclei of the mouse brain, such as the subventricular zone, a region capable of producing new neurons in the adult animal (Lois and Alvarez-Buylla 1993, Doetsch *et al* 1999, Quiñones-Hinojosa and Chaichana 2007).

In order to support the needs of such precision interventional techniques, an atlas that provides exact measures of vector deviations in a population of mice is required. To provide this capability, not available in existing atlases, we created a 3D atlas of the C57BL/6J mouse brain based on Paxinos and Franklin's *The Mouse Brain in Stereotaxic Coordinates* (Paxinos and Franklin 2001) that can be registered with and deformed to individual mouse MR data. The atlas and accompanying software allow the user to calculate and visualize local between-subject variability in morphology, data important for precision applications such as targeting of radiation delivery.

2. Methods and materials

2.1. Atlas generation

A schematic representation of our methods can be seen in figure 1. Digital images of the 100 slices of Paxinos' atlas of the C57BL/6J mouse brain (Paxinos and Franklin 2001) were downloaded from the CD-ROM accompanying the printed atlas. The gap between each slice varied from 0.12 mm to 0.36 mm. A software utility was written in C++ to pre-process the

atlas slices to ensure compatibility with the Pinnacle³ interface. Specifically, the atlas images were resized to 100 times their original size to facilitate triangular mesh generation because Pinnacle³'s mesh adaptation tools were not designed to operate on the scale of the murine brain. This operation did not compromise the quality of the image, as each image appears exactly as it does in Paxinos' atlas. Also, two blank slices were inserted between each existing slice to allow mesh structures that change dramatically between slices to be interpolated and thus to circumvent the problem of mesh discontinuity around contours that do not overlap from slice to slice. Finally, processed atlas images were output as a 300-slice raw image file readable by Pinnacle³ and at a decreased resolution to minimize data size. The Pinnacle³ environment used to manipulate atlas slices and to generate triangular meshes is demonstrated in figure 2. The processed atlas images were loaded into Pinnacle³, and automatic contouring tools followed by manual retouching were used to contour the following 18 structures: the external surface of the brain, the ventricular system (including the lateral ventricles, third ventricle, dorsal third ventricle, fourth ventricle and lateral recesses of the fourth ventricle) and features of the hippocampus (outer surface, dentate gyrus and subgranular zone). The final regions of interest (ROIs) were converted to a triangular mesh form by Pinnacle³ and exported to separate files in Visualization Tool Kit format (VTK, <http://www.vtk.org/>), ASCII text files containing a list of vertices in space that define a structure and a list of polygons (in our case triangles) connecting the vertices and defining the structure's surface, using custom scripts written in the Pinnacle³ scripting language.

2.2. Image acquisition

MR scans were acquired using a 9.4 T MRI BioSpec 94/20 (Bruker Inc., Billerica, MA). Scans were T2-weighted with the following parameters: TE = 25 ms, TR = 4000 ms, slice thickness = 0.5 mm, in-plane resolution = 0.0125 mm, field of view = 3.2 cm, with eight averages and a RARE factor of 4. Forty coronal slices were acquired in approximately 8 min. A 34 mm diameter coil was used.

2.3. Animals

We performed an animal study to create an atlas that better represents an average mouse than published histology atlases; we then compared this average atlas to the original structures in the histology atlas to quantify the differences. We used C57BL/6J mice of three different age groups: 5 weeks ($n = 3$), 8 weeks ($n = 7$) and 9 weeks ($n = 3$). All procedures were conducted with approval from the Johns Hopkins institutional Animal Care and Use Committee. Mice were immobilized in a custom in-house MR-compatible stereotactic head holder designed for the 30 mm coil (Matinfar *et al* 2009). This is similar to head holders developed by other groups (Fricke *et al* 2004, Kiehl *et al* 2008). Mice were anesthetized with a 2% mixture of isoflurane. The head holder bite block was designed to accommodate gas anesthesia.

2.4. Mesh adaptation

A combination of Pinnacle³ scripts and C++ software was used to load the histology-based atlas into a randomly selected MRI dataset; after mesh adaptation as described below, subsequent analyses were conducted using this template atlas (figure 1). The 3D structures of the atlas were manually translated and rotated as one entity to obtain a crude registration between the atlas and the MRI volume. The lateral ventricles were selected for analysis of deformations due to their high visibility in CT, MR and histology modalities; we did not use other features for our analysis due to their invisibility on *in vivo* imaging modalities. Once aligned with the volume, the lateral ventricle meshes were non-rigidly deformed to the volume using Pinnacle³'s model-based mesh adaptation tools, based on optimization of an energy function that attracts a structure to features of the target image data while penalizing

large deviations from the original model (Pekar *et al* 2004). The algorithm uses an image-based gradient search method to attract the mesh structure to regions of high contrast change. User-specifiable penalties prevent excessive deformation of the mesh, and a cost ensures that meshes will preferentially deform to closer gradient features. The total number of vertices in a structure is fixed because the software requires a starting value to initiate mesh generation since there are an infinite set of possible meshes, all with different numbers of vertices, that can describe a given shape. The mesh generation algorithm takes curvature into account, generating more vertices in regions of high curvature. The model-based adaptation procedure did not require recontouring of structures from the MRI volume. Once automatic adaptation was complete, the resulting meshes were refined with manual retouching of contours. The automatic adaptation settings were adjusted to search for a negative going gradient with more than 600 pixel values per mm and a weighting factor of 6 (0–10 scale) for the proximity of the gradient point relative to the current location of the mesh point. An organ flexibility weighting of 3 (0–10 scale) was used. Options to smooth and ‘clean’ ROIs after adaptation were disabled in order to maintain the number of mesh vertices. The resulting structures adapted to MRI volumes were exported using Pinnacle³ scripts to VTK format.

2.5. Average atlases

An affine transformation generated by an implementation of the iterative closest point algorithm (Besl and McKay 1992) within the MeshLab software package (available at <http://meshlab.sourceforge.net>) was used to register corresponding structures of each mouse age group in order to eliminate global differences in position. ParaView software (Kitware, Palo Alto, CA; available at <http://www.paraview.org/New/index.html>) was used to convert the adapted structures to the Stanford Polygon File Format for compatibility with MeshLab software and back to VTK format after registration. All corresponding structures within one mouse age group thus registered were combined into an average structure using C++ software in order to facilitate analysis of shape differences between the structures. We assumed a point-to-point correspondence during the deformation process, allowing the average atlas to be created by setting each vertex of the average structure equal to the vector mean of the corresponding points in its substituent structures. In this way, six average structures were created, consisting of left and right lateral ventricles for the 5-week-old, 8-week-old and 9-week-old cohorts.

2.6. Analysis of deformations

Individual structures were compared to their corresponding average structure using an in-house C++ software utility. The mean of the 3D vector distances between vertices in an individual structure and the corresponding vertices in the average structure, mean vertex deviation (MVD), is

$$\text{MVD}_{\text{MR-MR}} = \frac{\sum_{i=1}^n |\bar{X}_i - \bar{A}_i|}{n}$$

where \bar{X}_i is a vertex of the individual structure, \bar{A}_i is a vertex of the average structure derived from individual MR scans and n is the number of vertices of the structure in question (necessarily equal for individual and average structures).

MVD was illustrated as a color field mapped onto each individual structure by labeling each vertex with a color value proportional to the deviation of that vertex from the corresponding point in the average structure. The color fields were defined in our C++ code using existing

VTK color field capabilities and visualized in ParaView. The standard deviation and range of vertex deviations, as well as the volumes of each individual structure mesh and average mesh, were recorded.

2.7. Comparison to original histology atlas

A similar analysis technique was used to compare each individual structure mesh to the corresponding structure mesh from the original, non-deformed histology-based atlas. Mean vertex deviation in this case was calculated as follows:

$$\text{MVD}_{\text{MR-HIST}} = \frac{\sum_{i=1}^n |\bar{X}_i - \bar{H}_i|}{n}$$

where \bar{X}_i is a vertex of the individual structure and \bar{H}_i is a vertex of the histology-based structure. Mean vertex deviation was again mapped as a color field onto each individual structure, and the standard deviation and range of the vertex deviations were recorded.

2.8. Statistical analysis

$\text{MVD}_{\text{MR-MR}}$ with respect to all mice was compared with $\text{MVD}_{\text{MR-HIST}}$ with respect to all mice using separate, two-tailed paired Student's *t*-tests (one for each lateral ventricle). MVD and mean structure volume were also compared for both MR-MR and MR-HIST comparisons and for both lateral ventricles between immature (5-week-old) and mature (8- and 9-week-old) mice using two-tailed Student's *t*-tests for independent samples.

3. Results

3.1. Atlas generation

A 3D rendering of the atlas with selected structures visible is shown in figure 3. For visualization purposes, we added eyes to the histology atlas based on a randomly selected MR scan of an individual mouse registered to the histology atlas. Three-dimensional mesh structures generated by the Pinnacle³ software contained from approximately 500 to 6000 component triangles depending on the size and shape of the structure. For certain structures, the Pinnacle³ software was not able to generate a triangular mesh from the contours because of limited data present in Paxinos and Franklin's atlas; contours of white matter structures such as the corpus callosum and the external capsule did not overlap on consecutive atlas slices.

3.2. Adaptation to MR data

Figure 4 shows atlas structures of an individual mouse subject adapted to MR images. As a starting point, the Pinnacle³ software's model-based adaptation tools were used to deformably register the template atlas triangular meshes to each MR dataset. This atlas was subsequently used as a template, which was then adapted to each mouse's MR volume. Manual adjustments of the automatically adapted contours were made thereafter. In many cases, manual adjustment was required due to the lack of adequate contrast along the edges of the lateral ventricles in MR datasets. Table 1 describes the volume of MR-MR average and MR-histological structures created, as well as average volumes of individual mouse cohort structures.

3.3. Analysis of deformations

Table 2 describes the deformations calculated between individual MR-adapted meshes and the corresponding average structure for each group of mice. Mean and standard deviation of

vertex deviations were calculated as above. MVD values ranged from 0 mm to 0.457 mm over all mice. The average MVD of the three age groups ranged from 0.015 mm to 0.077 mm.

To aid in visualizing regions of extreme variability in individual structures, vertex deviations were mapped on to each individual subject mesh, as in figure 5. The color field was normalized to each left/right pair of individual subject structures.

The average volumes of the lateral ventricles over all mice in our study were 2.23 mm³ (left) and 2.17 mm³ (right), with a global average (both lateral ventricles) of 2.20 mm³. The difference in average volume between left and right lateral ventricles was not statistically significant.

3.4. Comparison to original histology atlas

Table 2 describes deviations calculated between individual MR-adapted meshes and the corresponding unadapted histology-based structure. Mean and standard deviation of vertex deviations were calculated as above. MVD values ranged from 0.002 mm to 0.728 mm over all mice. The average MVD values of the three age groups ranged from 0.054 mm to 0.091 mm.

Color maps of variability between structures were also created for the comparisons of individual subject structures to the original histology-based meshes. These color fields were also normalized to each left/right pair of individual structures.

3.5. Statistical analysis

MVD values between MR-adapted individual structures and their corresponding average structures were significantly less than MVD between MR-adapted individual structures and the corresponding original histology-based meshes (LLV: $p < 0.001$, RLV: $p = 0.004$).

There were no significant differences between MVD values by age group (5-week-old versus 8/9-week-old mice) or between lateral ventricle volumes by age group for either the MR-MR or the MR-HIST comparisons.

4. Discussion

The purpose of this study was to create a 3D histology-based atlas of the C57BL/6J mouse brain, deformable to MR data to enable precise atlas-based targeting of radiation and surgical procedures. We analyzed deviations in the structure of the lateral ventricles as a benchmark for the accuracy of our atlas and as a demonstration of the added precision conferred by deforming our initial, purely histology-based atlas to MR datasets. This analysis, while confirming the validity of our technique and demonstrating usefulness as a radiation or surgical targeting tool, also suggests that our technique has applications in phenotyping, morphometry and interventional studies, as previous phenotyping studies (e.g. Bock *et al* (2006)) relied on volumetric analysis to discover new phenotypic information. The approach outlined here may offer advantages over volumetric analysis and existing MR-based methods using local positional differences between mesh vertices as a gauge of structure variability, allowing for finer analysis of potentially new phenotypes, as well as over computed tomography (CT) studies where soft-tissue structures of interest are not delineable. Newer rodent irradiators (Wong *et al* 2008, Graves *et al* 2007, Jaffray *et al* 2006, Stojadinovic *et al* 2007) rely on CT guidance to deliver x-ray beams as small as 0.5 mm in diameter. However, some studies that may benefit from precise targeting often involve areas of the mouse brain that are not differentiable on CT or even on MR images, such as the subgranular zone of the dentate gyrus. This application would rely on features that are

distinguishable in CT images, such as the surface of the brain and the lateral ventricles to generate a deformation field from which the positions of structures not visible in CT images, such as the dentate gyrus, can be interpolated, thereby enabling targeting of these regions. In addition, validating our atlas using white matter structures that are visible in imagery presented a difficulty in that the high aspect ratio and small scale in mice of these structures were not compatible with mesh generation in Pinnacle³. This represents an avenue for further development, as modifications to the mesh generation algorithm might support meshing of such structures.

4.1. Advantages of an *in vivo* MR-deformable histology-based atlas

It has been shown that subtle changes, detectable by high-resolution MR, in the volume of small anatomical structures in the mouse brain can be indicative of pathological changes (Cyr *et al* 2005), and that *in vivo* MR-based volumetric analysis is powerful enough to characterize neuroanatomical mutant phenotypes (Bock *et al* 2006). However, detailed analysis of structural variability would presumably be an even more powerful metric than simple calculations of volume in certain phenotypes. The ability of our approach to calculate and visualize individual structure variability is not available in atlases based on analysis of regional changes in surface (Ma *et al* 2005) and volume (Kova evi *et al* 2005). In the latter study, structure variability is quantified by calculating a ‘mean positional difference’, viewable as a color field mapped onto the average image. The regions of the mouse brain with greatest variability, as identified by that group, are those affected most by the preparation procedures, such as the brain stem and the olfactory bulbs, subject to damage during excision (Kova evi *et al* 2005). This unavoidable consequence of *ex vivo* MR scans of excised specimens renders phenotyping of such structures impossible and skews the distribution of deviations toward large distances.

Our study extends the morphometric capabilities of Kova evi *et al*'s (2005) atlas, as our approach begins with an accurate high-resolution collection of structures based on histology and then adapts this to specimens *in vivo*. In addition, each structure can be examined separately since the structures are represented by their own triangular meshes. Thus, structures can be compared both *in situ* by registering the whole brains of mice to be compared (for use in surgical or radiation treatment targeting) and *ex situ* by comparing only the structures of interest. In both cases, differences on the vertex level can be calculated and visualized as color fields. A future application of this method would be an automated procedure by which individual structures could be compared both *in situ* and *ex situ*, regions of high variability could automatically be flagged, representing a much faster approach to finding and characterizing mutants in phenotyping studies.

A similar application is suggested by Badea *et al* (2007) using the atlas developed in that laboratory, capable of local morphometric analysis of individual brain structures. However, the data on which the 3D atlas in that study was based were compiled by creating an average MR dataset and using automated segmentation to derive structure boundaries, as in other studies (Ma *et al* 2005, Chen *et al* 2006). Not only is this method computationally intensive, calculation of an average image may not preserve the detail of highly variable structures such as white matter tracks in the 3D atlas (Kova evi *et al* 2005). Our approach uses the semiautomated model-based adaptation system in the Pinnacle³ software to deform an accurate histology-based mesh onto MR images, a relatively fast (one lateral ventricle in an individual mouse subject can be adapted in less than 10 min) and accurate process. Our approach is faster because it relies on a small number of vertex points (<6000) to calculate average structures rather than deformation of images (e.g. Ma *et al* (2005)). One limitation of our approach currently is in the definition of long and thin structures such as the corpus callosum where contours from consecutive slices do not necessarily overlap. One possible

future solution may be to add more interpolating slices to generate a smoother starting structure.

4.2. Calculations of volume and variability

We calculated a global average volume for the mouse lateral ventricles of 2.23 mm^3 (left) and 2.17 mm^3 (right). This result closely mirrors published findings (Dorr *et al* 2008) of $2.0 \pm 0.83 \text{ mm}^3$ (left) and $2.1 \pm 0.50 \text{ mm}^3$ (right) for 12-week-old male C57BL/6J mice, obtained from that group's high-resolution ($32 \mu\text{m}$ isotropic voxels) MR-based atlas of 20 male and 20 female mice.

Kova evi *et al* (2005) found that the majority of points in individual MR images of mice never varied more than $117 \mu\text{m}$ from the corresponding points in their atlas' average image. While $\text{MVD}_{\text{MR-MR}}$ values for individual mice in our study are as great as 0.457 mm , global average $\text{MVD}_{\text{MR-MR}}$ values for the lateral ventricles over all mice were 0.044 mm (left) and 0.045 mm (right). The finding that both MVD values and calculated volumes parallel published findings suggests that we have developed an atlas capable of accurate morphometry of the C57BL/6J brain.

Values of $\text{MVD}_{\text{MR-HIST}}$ were significantly greater than $\text{MVD}_{\text{MR-MR}}$ values, with global averages of $\text{MVD}_{\text{MR-HIST}}$ for lateral ventricles of 0.082 mm (left) and 0.068 mm (right). In other words, individual MR-adapted structures are more similar to an MR-based average structure than they are to the original histology-based structures. This suggests that our technique represents a more accurate method of modeling C57BL/6J anatomical structures than simply applying a 3D representation of a histology-based atlas alone. Refinement of our atlas with data from more mice of a wider age range would not only improve the validity of our findings, but may also shed light on morphometric differences in C57BL/6J brain anatomy between mice of different ages, a subject that has not, to our knowledge, been previously studied.

References

- Amunts K, Zilles K. Advances in cytoarchitectonic mapping of the human cerebral cortex. *Neuroimaging Clin North Am.* 2001; 11:151–69.
- Badea A, Ali-Sharief AA, Johnson GA. Morphometric analysis of the C57BL/6J mouse brain. *NeuroImage.* 2007; 37:683–93. [PubMed: 17627846]
- Besl PJ, McKay ND. A method for registration of 3-D shapes. *IEEE Trans Pattern Anal Mach Intell.* 1992; 14:239–56.
- Bock NA, Kova evi N, Lipina TV, Roder JC, Ackerman SL, Henkelman RM. *In vivo* magnetic resonance imaging and semiautomated image analysis extend the brain phenotype for cdf/cdf mice. *J Neurosci.* 2006; 26:4455–9. [PubMed: 16641223]
- Chen XJ, Kova evi N, Lobaugh NJ, Sled JG, Henkelman RM, Henderson JT. Neuroanatomical differences between mouse strains as shown by high-resolution 3D MRI. *NeuroImage.* 2006; 29:99–105. [PubMed: 16084741]
- Cyr M, Caron MG, Johnson GA, Laakso A. Magnetic resonance imaging at microscopic resolution reveals subtle morphological changes in a mouse model of dopaminergic hyperfunction. *NeuroImage.* 2005; 26:83–90. [PubMed: 15862208]
- Doetsch F, Caillé I, Lim DA, García-Verdugo JM, Alvarez-Buylla A. Subventricular zone astrocytes are neural stem cells in the adult mammalian brain. *Cell.* 1999; 97:703–16. [PubMed: 10380923]
- Dorr AE, Lerch JP, Spring S, Kabani N, Henkelman RM. High resolution three-dimensional brain atlas using an average magnetic resonance image of 40 adult C57Bl/6J mice. *NeuroImage.* 2008; 42:60–9. [PubMed: 18502665]

- Eickhoff S, Walters NB, Schleicher A, Kril J, Egan GF, Zilles K, Watson JDG, Amunts K. High-resolution MRI reflects myeloarchitecture and cytoarchitecture of human cerebral cortex. *Hum Brain Mapp.* 2005; 24:206–15. [PubMed: 15543596]
- Fricke ST, Vink R, Chiodo C, Cernak I, Ileva L, Faden AI. Consistent and reproducible slice selection in rodent brain using a novel stereotaxic device for MRI. *J Neurosci Methods.* 2004; 136:99–102. [PubMed: 15126050]
- Graves EE, et al. Design and evaluation of a variable aperture collimator for conformal radiotherapy of small animals using a microCT scanner. *Med Phys.* 2007; 34:4359–67. [PubMed: 18072501]
- Jaffray D, et al. An image-guided irradiator for pre-clinical radiation therapy studies. *Med Phys.* 2006; 33:2241.
- Kiehl EL, et al. Feasibility of small animal cranial irradiation with the microRT system. *Med Phys.* 2008; 35:4735–43. [PubMed: 18975718]
- Kovačević N, et al. A three-dimensional MRI atlas of the mouse brain with estimates of the average and variability. *Cereb Cortex.* 2005; 15:639–45. [PubMed: 15342433]
- Lois C, Alvarez-Buylla A. Proliferating subventricular zone cells in the adult mammalian forebrain can differentiate into neurons and glia. *Proc Natl Acad Sci USA.* 1993; 90:2074–7. [PubMed: 8446631]
- Ma Y, et al. A three-dimensional digital atlas database of the adult C57BL/6J mouse brain by magnetic resonance microscopy. *Neuroscience.* 2005; 135:1203–15. [PubMed: 16165303]
- Matinfar M, Ford E, Iordachita I, Wong J, Kazanzides P. Image-guided small animal radiation research platform: calibration of treatment beam alignment. *Phys Med Biol.* 2009; 54:891–905. [PubMed: 19141881]
- Paxinos, G.; Franklin, KBJ. *The Mouse Brain in Stereotaxic Coordinates.* 2. San Diego, CA: Academic; 2001.
- Pekar V, McNutt TR, Kaus MR. Automated model-based organ delineation for radiotherapy planning in prostatic region. *Int J Radiat Oncol Biol Phys.* 2004; 60:973–80. [PubMed: 15465216]
- Quiñones-Hinojosa A, Chaichana K. The human subventricular zone: a source of new cells and a potential source of brain tumors. *Exp Neurol.* 2007; 205:313–24. [PubMed: 17459377]
- Stojadinovic S, et al. MicroRT—small animal conformal irradiator. *Med Phys.* 2007; 34:4706–16. [PubMed: 18196798]
- Toga AW, Smaie M, Payne BA. Digital rat brain: a computerized atlas. *Brain Res Bull.* 1989; 22:323–33. [PubMed: 2706541]
- Wong J, et al. High-resolution, small animal radiation research platform with x-ray tomographic guidance capabilities. *Int J Radiat Oncol Biol Phys.* 2008; 71:1591–99. [PubMed: 18640502]
- Zhao C, Deng W, Gage FH. Mechanisms and functional implications of adult neurogenesis. *Cell.* 2008; 132:645–60. [PubMed: 18295581]

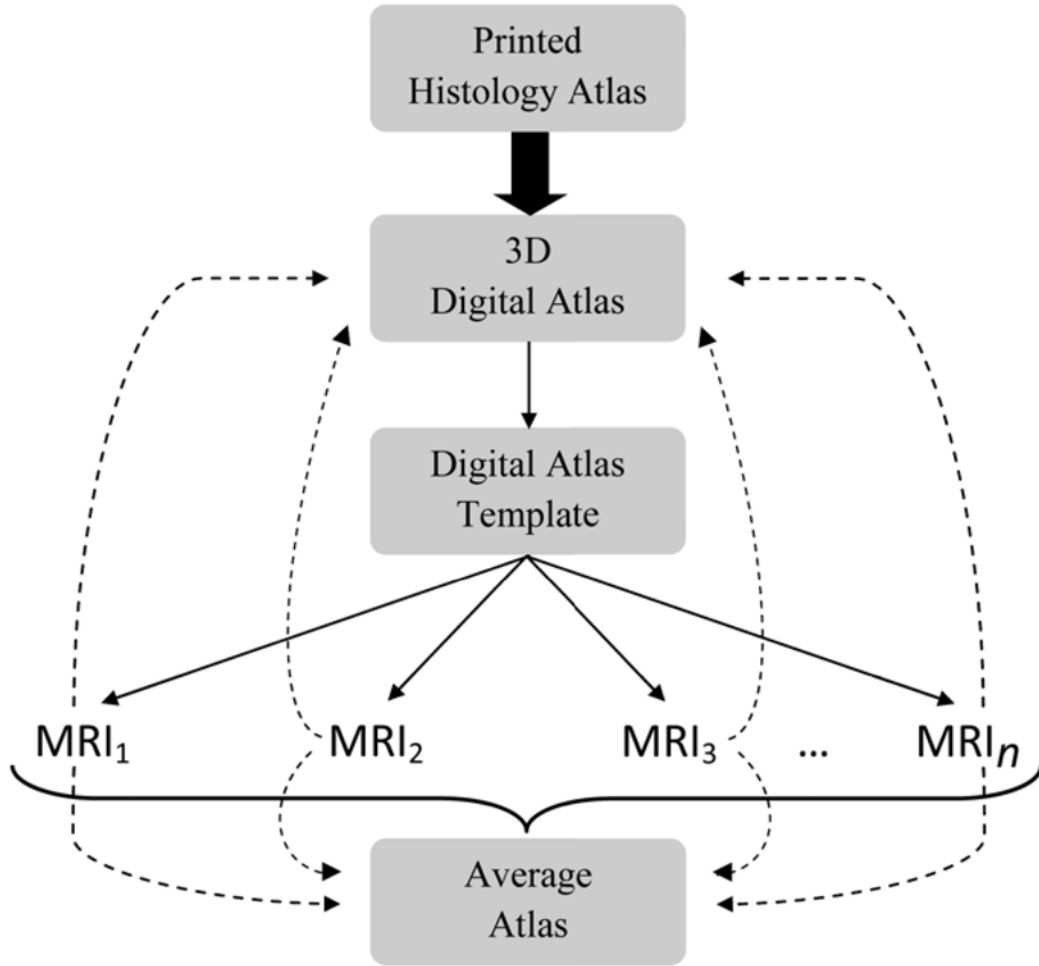


Figure 1. Schematic representation of the processes involved in triangular mesh generation from the original histology atlas, adaptation to individual mouse MRI, creation of an average atlas (based on a single age cohort) and comparison of individual MRI to both original histology structures and new average atlas structures. The printed histology atlas was converted to a three-dimensional, digital atlas using mesh generation tools in Pinnacle³ (thick arrow). A template digital atlas (adapted to a randomly selected mouse’s MRI volume using the methods described above) was then registered and adapted to individual mouse MRI volumes in an age cohort (represented as MRI₁, MRI₂, etc; adaptation represented by thin solid arrows). Structures from the digital atlas adapted to individual mouse MRI were then combined into an average atlas (bracket), which was then compared to both individual mouse structures and to the original histology atlas (dashed arrows).

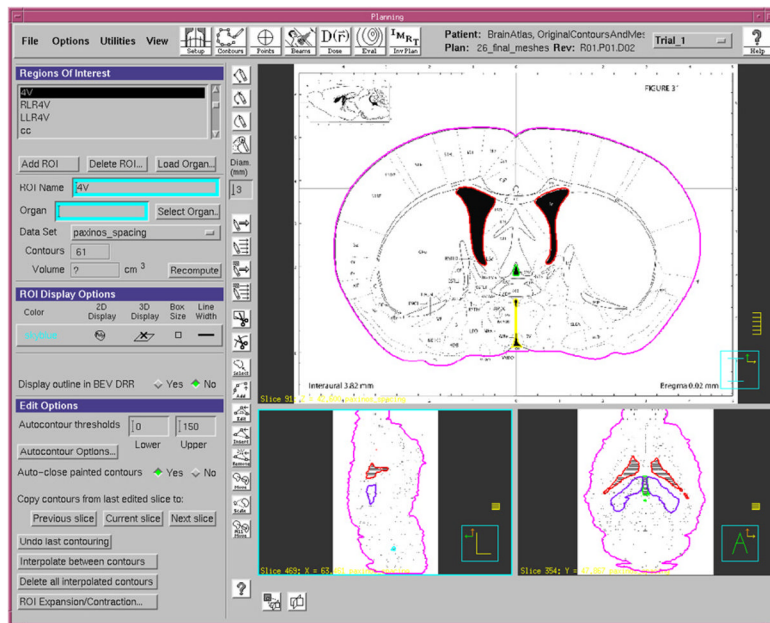


Figure 2. The Pinnacle³ radiation therapy planning software interface during mesh generation. The right side of the interface screen shows orthogonal views of the digital versions of slices of Paxinos and Franklin's mouse brain atlas (Paxinos and Franklin 2001). Regions of interest (ROIs) corresponding to the outer surface of the brain (magenta), lateral ventricles (red), dorsal third ventricle (green), third ventricle (yellow), fourth ventricle (blue) and hippocampus (purple) are displayed.

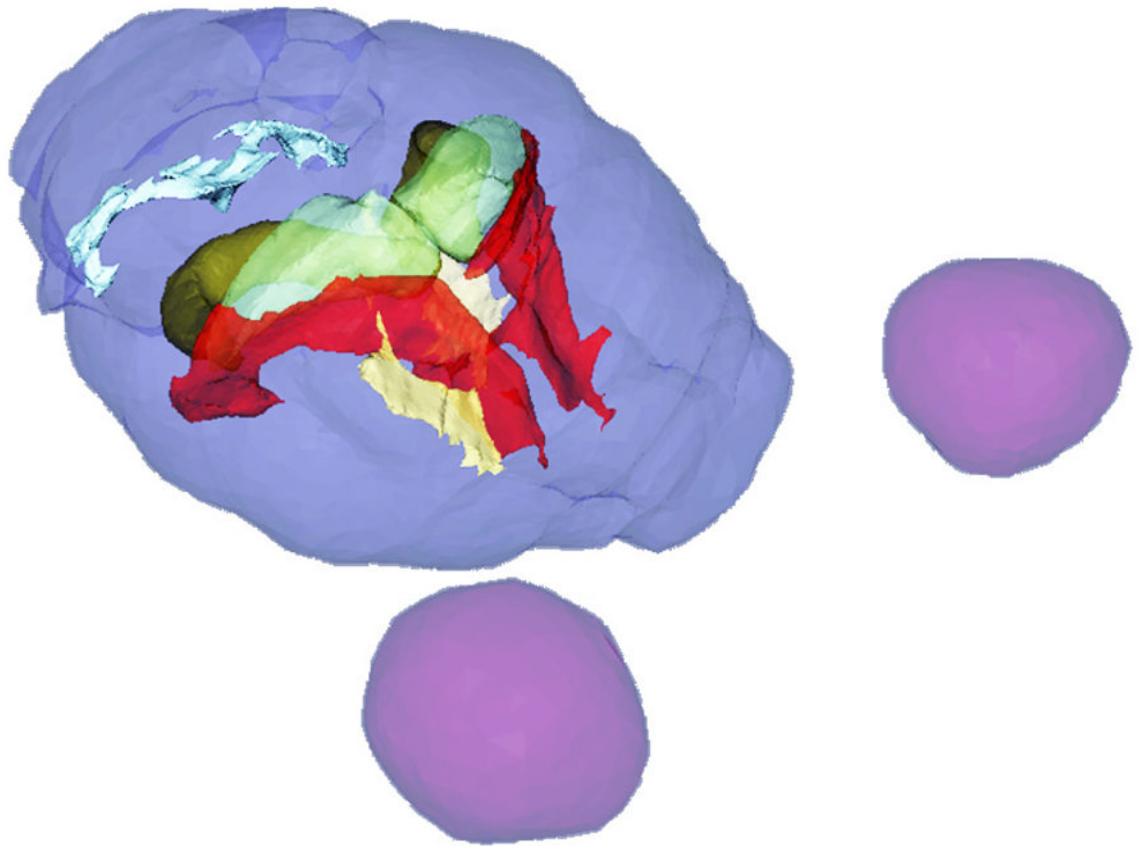


Figure 3.

Three-dimensional rendering of the histology-based mouse brain atlas. Structures visible are eyes (added from an MR dataset for reference; purple), brain surface (dark blue), lateral ventricles (red), third ventricle (yellow), fourth ventricle (light blue), anterior region of hippocampus (light green) and dentate gyrus (dark green).

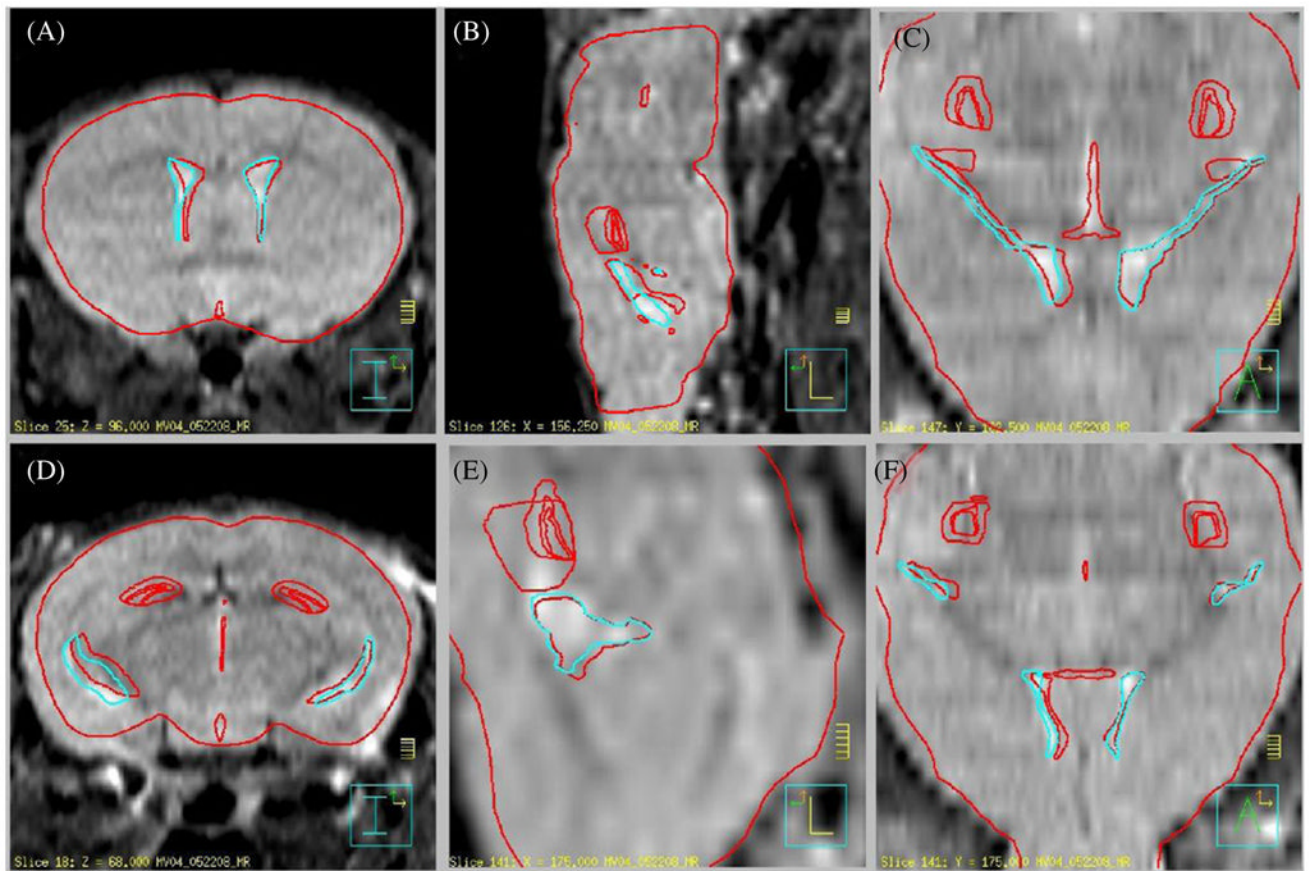


Figure 4.

Typical adaptation of crudely aligned histology-based 3D mesh structures (red) with MR images of a single individual mouse subject in coronal (A, D), sagittal (B, E) and axial (C, F) views. Semi-automatically adapted mesh structures are visible in blue. In this example, original histology structures (red) are manually registered with the MRI. Only lateral ventricles are adapted (blue). No attempt is made to adapt the brain surface, as the brain surface was not of anatomical interest.

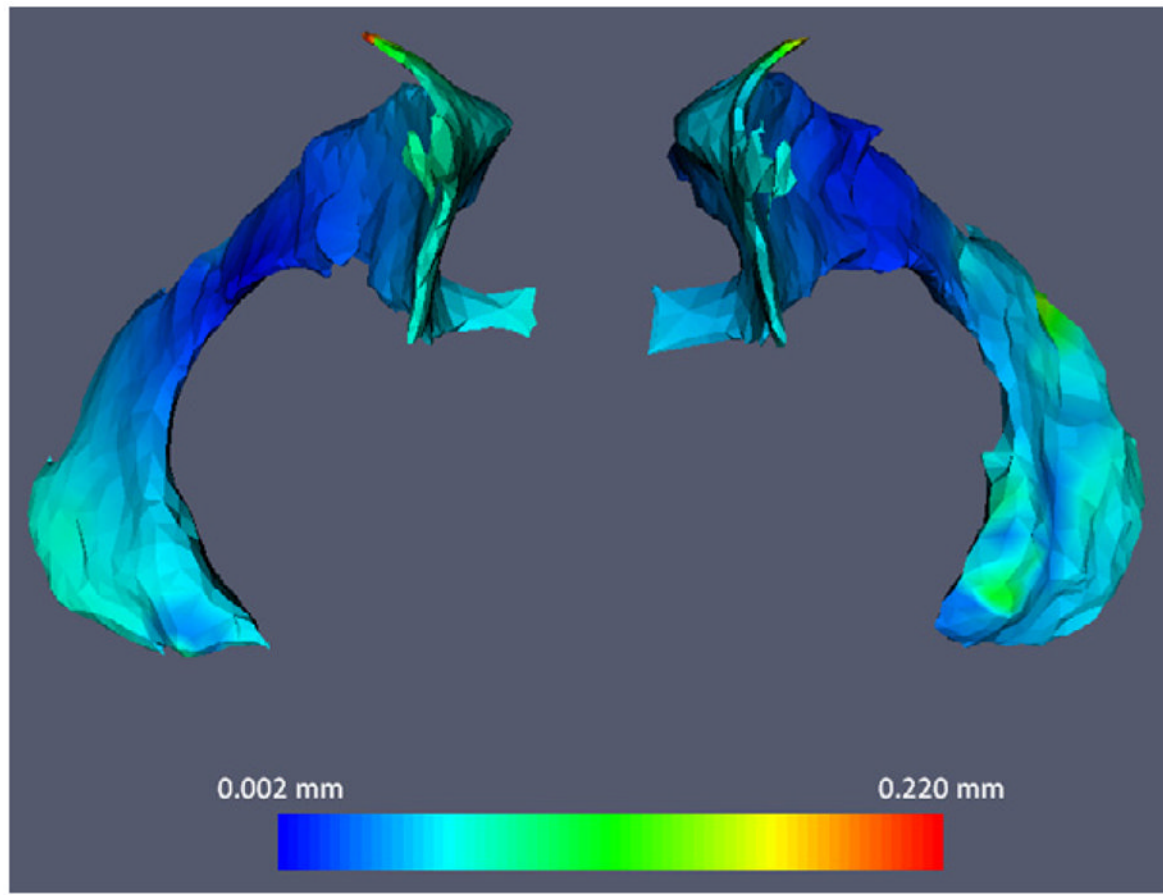


Figure 5. Vertex deviations of an individual 8-week-old mouse subject's lateral ventricles versus the average lateral ventricle meshes for the 8-week-old cohort ($n = 7$) displayed as a colour field. The projection aspect represents a view down along the rostral–caudal axis.

Table 1

Volumes of MR-MR average atlas structures and histology-based atlas structures.

Age (weeks)	Structure	n	Mean vol (mm ³)	SD vol (mm ³)	Vol of Avg Struct (mm ³)	Vol of His Struct (mm ³)
5	LLV	3	2.01	0.227	2.00	2.06
5	RLV	3	2.16	0.080	2.15	2.02
8	LLV	7	2.33	0.202	2.32	2.06
8	RLV	7	2.18	0.265	2.17	2.02
9	LLV	3	2.22	0.007	2.22	2.06
9	RLV	3	2.16	0.267	2.15	2.02
Global Avg	LLV	13	2.23	0.234	–	–
Global Avg	RLV	13	2.17	0.246	–	–

Mean vol = mean volume of individual structures of a cohort; SD vol = standard deviation of volumes of individual structures of a cohort; Vol of Avg Struct = volume of the average structure generated from the corresponding individual structures in a cohort; Vol of His Struct = volume of the original mesh generated from Paxinos' histology atlas.

Table 2

Comparison of individual MR-adapted structures to MR-based average structures and original histology-based structures.

Age (weeks)	Structure	n	MVD _{MR-MR} (mm)	SD VD _{MR-MR} (mm)	MVD _{MR-HIST} (mm)	SD VD _{MR-HIST} (mm)
5	LLV	3	0.077	0.056	0.082	0.055
5	RLV	3	0.031	0.024	0.054	0.042
8	LLV	7	0.043	0.040	0.091	0.047
8	RLV	7	0.048	0.040	0.071	0.048
9	LLV	3	0.015	0.016	0.062	0.032
9	RLV	3	0.050	0.033	0.076	0.034
Global Avg	LLV	13	0.044	0.030	0.082	0.036
Global Avg	RLV	13	0.045	0.026	0.068	0.031

MVD_{MR-MR} and SD VD_{MR-MR} = mean and standard deviation of vertex deviations between individual structures in a cohort and the corresponding average structure; MVD_{MR-HIST} and SD VD_{MR-HIST} = mean and standard deviation of vertex deviations between individual structures in a cohort and the corresponding histological structure; Global Avg = values of MVD_{MR-MR}, SD VD_{MR-MR}, MVD_{MR-HIST} and SD VD_{MR-HIST} averaged over all mice regardless of age cohort.